JOURNAL OF SPACECRAFT AND ROCKETS
Vol. 31, No. 3, May–June 1994

Arcing of Negatively Biased Solar Cells in a Plasma Environment

B. L. Upschulte,* W. J. Marinelli,† and K. L. Carleton*
Physical Sciences, Inc., Andover, Massachusetts 01810
G. Weyl‡
Network Physics, Lexington, Massachusetts 02173
E. Aifer§
Boston University, Boston, Massachusetts 02215
and
D. E. Hastings¶
Massachusetts Institute of Technology, Cambridge, Massachusetts 02139

Experimental and theoretical efforts have been conducted to investigate the arcing of negatively biased solar arrays in a low-Earth orbit plasma environment. Experiments were conducted in an ultrahigh vacuum plasma test chamber, where the environment could be controlled carefully. Outgassing of the adhesive used to bind the protective coverglass to the solar cells was determined to be a key factor in observed arcing rates. These rates could be reduced by greater than a factor of 100 by eliminating or fully outgassing the excess adhesive remaining at the edge of the solar cells. Optical emission from solar cell arcs was observed to correlate linearly with arc current, both temporally and in total intensity. Solar cell arcing rates were also observed to scale linearly with plasma density. The plasma scaling is in good agreement with a theory based on enhanced field electron emission charging of dielectric surfaces, leading to enhanced electric fields at the conductor/adhesive/plasma triple junction. Apparent thresholds for solar cell arcing are reported.

I. Introduction

IN conventional solar array power systems, cells with a bandgap of approximately 1 V are connected in series to achieve an array voltage of 32 V, which is regulated to a constant 28-V level. A large assembly of these arrays, connected in parallel, are used to meet the power requirements of large space vehicles. Significant weight savings can be obtained by operating these arrays at higher voltages. Interaction of the high-voltage ends of the arrays with the ambient space plasma found in low-Earth orbit (LEO) may lead to surface snapover for positively biased components and arcing in negatively biased components. Although these events may damage the arrays, the adverse effects are first observed as interruptions or resets of sensitive spacecraft electronics, digital processors, and communications systems. Typically, solar cell arrays are operated with the negative end of the array attached to the vehicle structural ground. Enhanced electron capture by the positive end of the array causes the majority of the array and grounding structure to float at high negative potentials with respect to the plasma.

In this paper we will address the operation of solar cells biased at negative high voltages (corresponding to a negative ground configuration). Experiments conducted on the PIX I and PIX II experiments showed that the arc frequency for negatively biased cells was dependent on both the bias voltage and plasma density.[1-3] Numerous experiments[4-13] conducted in space plasma simulation chambers using negatively biased cells of similar construction have noted the occurrence of several common phenomena: 1) an apparent threshold for arcing near −200 V and a steep dependence of the arc rate on bias voltage, 2) a conditioning of the cells manifested as an initially high arc rate that then decreased to a constant level in time, and 3) a propensity for the cells to arc at "triple junctions" occurring at the interconnect region or along the cell/coverglass interface.

Theoretical modeling and detailed experimental investigations, like this one, are just beginning to address the mechanisms that control these phenomena and previous observations. Two distinct mechanisms are advanced to explain the propensity for arcing in these arrays. Dielectric breakdown of a thin layer of insulating contaminant covering the metallic interconnect has been proposed by Parks et al.[14] to explain arc initiation. In a plasma environment, ions are attracted to the surface of the contaminant layer by the negative potential of the underlying interconnect, neutralizing the layer's surface. The large internal fields generated across the contaminant layer lead to emission across the interface and vaporization of the contaminant. The discharge is sustained via electron ionization of the vaporized layer. Hastings et al.[15] and Weyl et al.[16] have proposed that arcs are generated by the desorption and ionization of neutral molecules from the surface of the coverglass as a result of electron emission from the interconnect. The available experimental evidence is insufficient to verify either theory.

The efforts described in this paper seek to discover and mitigate the fundamental processes that are responsible for arcing and, to a lesser extent, parasitic current collection. The approach is twofold, with an experimental investigation of these processes coupled to a theory and modeling effort. The experimental efforts focused on two issues: 1) the arcing of negatively biased solar cells placed in an LEO plasma environment and 2) the behavior of Dow Corning DC93-500 adhesive under plasma exposure. This adhesive is used to bond the protective coverglass to the solar cells. During the investigation of the arcing of solar cells, it became apparent that the interaction

Received Oct. 30, 1992; revision received April 10, 1993; accepted for publication April 10, 1993.

*Principal Scientist, 20 New England Business Center.
†Thermophysic Area Manager, 20 New England Business Center. Member AIAA.
‡23 Somerset Road.
§Research Associate, Electrical and Computer Systems Engineering Department, 444 Cummington Street.
¶Professor, Department of Aeronautics and Astronautics, 77 Massachusetts Avenue. Member AIAA.

of DC93-500 adhesive with the space plasma and ambient environment was a key factor in determining arcing rates.

II. Experimental Investigations of Solar Cell Arcing

There have been numerous laboratory investigations of both solar cell arcing and parasitic current collection under negatively biased conditions in an LEO plasma environment.[4-14] In contrast, there have been significantly fewer flight investigations. In general, the major difference between the two types of measurements has been the use of relatively high-density rare gas plasmas (10^5 to 10^6 ions cm^{-3}) in laboratory systems compared with the much lower density, largely oxygen plasmas (10^3 to 10^5 ions cm^{-3}) found in LEO. Given the apparent scaling of arc rate with plasma density obtained in the PIX II flight data as well as differences between the preflight ground test and flight data for the PIX II array,[3] the validity of ground testing for these systems is constantly at issue. This situation is aggravated by the sparse and often compromised quality of the flight data.

A. Approach

Our measurements were not targeted at measuring accurate arcing rates for specific array configurations; i.e., quantitative comparison with flight data was not a primary goal of the effort. Previous work on the theory of arcing[15,16] had indicated that surface contaminants and microscopic surface structures might play a role in arc initiation and maintenance. Hence, a primary goal of this effort was to conduct arcing measurements under conditions where surface composition, structure, and contamination could be controlled and verified.

Early in the performance of these measurements, three issues arose concerning the reporting of arcing phenomenon: 1) how to define an arc, 2) how to measure an arcing threshold, and 3) how to define the appropriate conditions for making arcing measurements. Our experiments in general noted that solar cell discharge phenomenon fell into two regimes. One regime was characterized by frequently occurring discharges, short in duration (~ 50 ns), which dissipated little charge and had an immeasurable impact on the measured cell voltage. These current pulses are similar to the current surges observed before breakdown of electrical insulation.[17] Interspersed with these small arcs (or pre-arcs) were larger events, 1–5 μs in duration, which transferred significant amounts of charge from the array to the surrounding plasma and resulted in a significant (> 5%) reduction in the cell voltage. The shorter arcs produced no detectable optical emission, whereas, as will be seen, optical emission from the larger arcs could be directly correlated with the amount of charge dissipated. We chose as an operational definition of an arc one in which the observed voltage drop was greater than 5% of the bias voltage and where optical emission was detectable.

An important issue in the performance of the experiments was the setting of a threshold for the arcing process. For there to be a true threshold for the arcing process, there would have to be a part of the process that was energetically unfavorable below a given bias voltage, such as sputtering or secondary electron emission. In the laboratory, or in a flight experiment, one measures arcing rates and seeks to find a voltage below which arcing is never observed. Ferguson[3] has provided an operational definition of a threshold that uses an extrapolation of the observed arc rate from higher voltages. The threshold is attained when the measured arc rate falls three standard deviations below the arc rate extrapolated from high voltages. In practice, arcing rates become negligible as one approaches the −100- to −300-V regime, with the time between arcs approaching the available measurement time. Furthermore, the definition presumes a common mechanism for arc initiation throughout the entire voltage range.

The use of larger arrays to measure arcing rates at low voltages could, in principle, improve the measurements by increasing the number of arc sites. However, in practice arcs from different parts of the array are correlated through depletion of surface charge on large parts of the array from an arc occurring at a single site. In low plasma density environments it is likely that the arc rate is determined by the recharge rate of the array dielectric surfaces and the arcing rate of the site with the lowest threshold. Hence, measurements of arc thresholds are much more likely to reflect the ability of the experimenter to count low arc rates than the discovery of a true threshold. Our efforts focused instead on changes in the cell design or processing that could have a significant impact on the measured arc rate.

Many researchers have noted a reduction in cell arc rates over time at a specific bias voltage or a conditioning of the cell. In general, the rate of conditioning is accelerated at higher bias voltages. Our approach to avoiding these artifacts has been to condition the cells at −1000-V bias until the arc rate stabilizes at a fixed value. Then, our arc rates are measured at a lower absolute value of the bias voltage.

B. Experimental Apparatus

All experiments were conducted in a turbomolecular-pumped ultrahigh vacuum chamber. The chamber is a 21-in.-long by 10-in.-o.d. cylinder with all ports sealed with Cu gaskets and knife edge flanges to allow operation at pressures as low as 2×10^{-11} Torr. The chamber is shown schematically in Fig. 1. An Auger electron spectrometer may be positioned to within 0.25 in. of the sample for surface analysis. A differentially pumped quadrupole mass spectrometer (0–300 amu range) is configured to detect species desorbed from the sample as well as the background environment. An endwall port is used for optical measurements and may be equipped with a fast, low-resolution optical spectrometer for discharge characterization. The samples to be tested are mounted in the cradle of a 5 degree-of-freedom UHV sample manipulator. A Kaufmann-type, charge-neutralized ion plasma source is mounted on a vacuum flange and slides into a full nipple extension attached to an 8-in. conflat port on the UHV chamber. Planar and cylindrical Langmuir probes are mounted on translational stages, as shown in Fig. 2. The planar probe consisted of a 3.8-cm-diam copper disk, whereas the cylindrical probe had a length of 2.34 cm and a width of 0.25 mm and was oriented parallel to the incoming ion flow.

Most of the samples tested were positioned 34 cm downstream from the source. The radial profile of the ion beam was obtained from a measurement of the ion saturation current using the cylindrical probe. The beam is observed to have a diameter of roughly 5 cm at half maximum density. At ion extraction energies less than 40 eV, the electron temperature was found to be 1.25 eV ± 0.15 eV, and the ion energy spread was 7.5

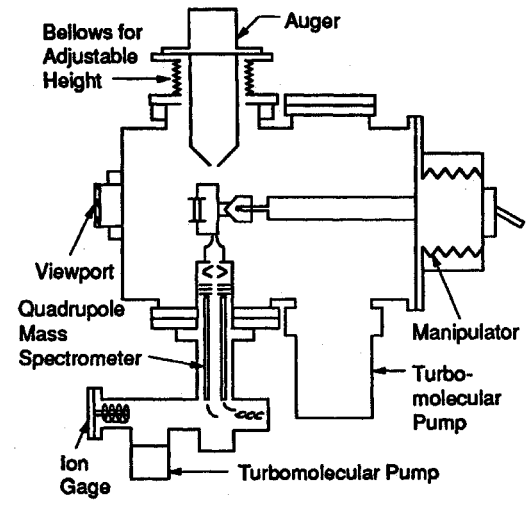

Fig. 1 Schematic drawing of the UHV chamber showing location of diagnostics.

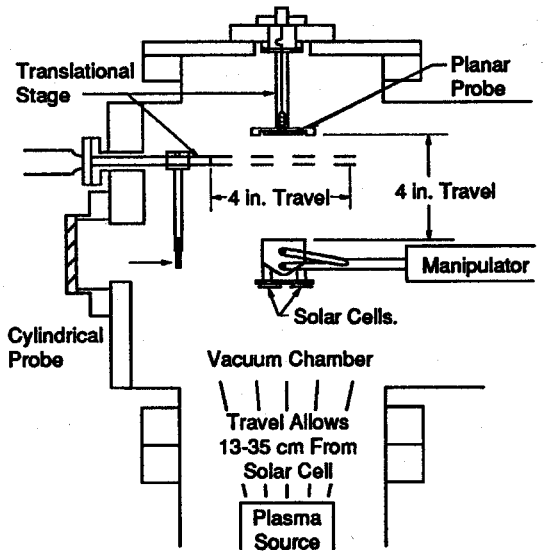

Fig. 2 Langmuir probe and solar cell mounting in UHV chamber.

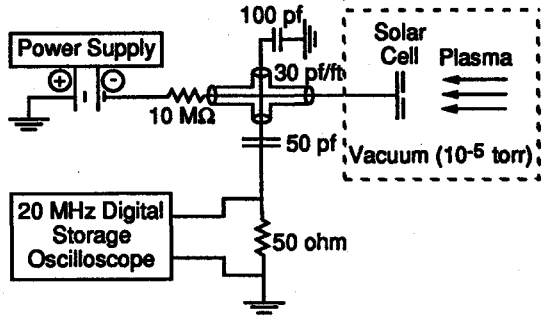

Fig. 3 Schematic for arc sensor circuit.

eV. Standard plasma source conditions were defined for all of the arc test series. The beam energy was 20 eV, the source to interconnect distance was 34 cm, and the ion saturation current was roughly 7×10^{-7} A/cm^2.

C. Electrical Diagnostics

Samples were placed in the UHV chamber and mounted onto a Kovar plate that could be biased negatively with respect to the chamber walls and the ion beam. The biasing circuit and arc sensing circuit are shown in Fig. 3. Design and construction of the arc sensing circuit are based on an experiment schematic by Snyder.[7] The data acquisition system used to record the arc time evolution is a Health Zenith PC-based 20-MHz real-time digital storage oscilloscope. The oscilloscope A/D channel senses a voltage drop across the 50-Ω resistor as charge stored in the capacitors flows to the arc site. The time constant of the sensor is determined by the RC product of the 50-Ω resistor and the 50-pF capacitor in series, i.e., 2.5 ns. For measuring arc characteristics that have durations of a few microseconds (1–10), this is an adequate response time. The recharge time of the arc-depleted interconnect by the power supply is controlled by the 10-MΩ resistor, 100-pF capacitor, and series associated cable capacitance. This recharge time constant is on the order of 1 ms and thus does not contribute to observations made of the arc event in the 1-μs time frame. The voltage drops across the 50-Ω resistor actually arises due to only a fraction of the current drawn by the arc. This fraction corresponds to 50 pF divided by the total capacitance in the system beyond the 10-MΩ resistor and is approximately 0.1. The change in bias voltage on the cell was recorded using a Tektronix model P6015 high-voltage probe. This probe provides a 1000 to 1 attenuation of the (ac/dc) voltage with a better than 8-MHz bandwidth.

D. UV Radiometer

A UV radiometer, consisting of a Hamamatsu model R1220 solar blind photomultiplier tube, was employed to observe emission of light from the array test region. This tube has response from 115 to about 305 nm with a ~0.2 quantum efficiency. The air transmission cutoff at around 190 nm sets the lower wavelength bound. During the experiment, the radiometer was positioned at a quartz vacuum window 6 in. from the solar cell. The signal from the radiometer passes to the computer scope.

E. Optical Multichannel Analyzer Spectrometer

A Princeton Instruments optical multichannel analyzer (OMA) coupled to a Jarrell-Ash 1/4-m monochromator was used to view and spectrally disperse emission from arc events in the 200–400-nm region. Spectra comprised of multiple arcs were recorded by gating the OMA, with an exposure time of 5 μs, as triggered by the output of the arc sensor.

F. Intensified Array Camera

Images of individual arc events between the solar cell and the plasma were captured on the gated and image-intensified CCD camera system that permits asynchronous control of the camera and synchronization with the trigger source from the arc sensor. The intensifier is gated on coincidentally with the trigger pulse for 5 μs to capture the arc emission while eliminating unwanted background light. For this application the camera was coupled to a Nikon F/4.5 compound CaF_2 lens system and a UG-5 uv transmitting filter to minimize the unwanted visible glow of the hot tungsten filament.

G. Solar Cell Test Samples

Solar cell arcing tests were performed primarily on single 1×2 cm^2 silicon cells supplied by Spectrolab Inc. A schematic diagram of the silicon cell construction is shown in Fig. 4. The cell is comprised of a 150-μm-thick AR-coated fused silica coverglass attached to a 64-μm-thick silicon cell with Dow Corning DC93-500 two-part RTV adhesive. This adhesive is a low-volatility type that has been extensively characterized in connection with spacecraft contamination studies.[18] The coverglass extends over the edge of the silicon cell on three sides by approximately 100 μm. A metallized interconnect tab is connected to the cell along the 2-cm edge for current extraction. The coverglass terminates where the current collection tab leaves the cell surface. A thin film of adhesive acts as a buffer between the tab and the edge of the coverglass. The base of the cell is coated with a multilayer metallization for bonding to the metallized tab on the next cell in the array series.

Figure 5 shows an expanded view of the underside of a typical solar cell, where the coverglass extends over the silicon cell edge, taken using a reverse contrast microscope. The black regions of the photograph show where excess DC93-500 adhesive has extruded from beneath the cover slip during fabrication. The adhesive has formed a jagged and somewhat irregular seal along the edge of the silicon. A recent inspection of the array edges on the SSF 8×8 cm^2 cells has shown approximately 70% of the cell edges are obscured by the excess adhesive.[19]

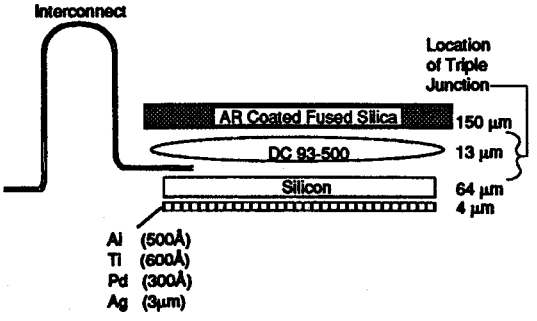

Fig. 4 Schematic diagram of 1×2 cm^2 solar cell construction.

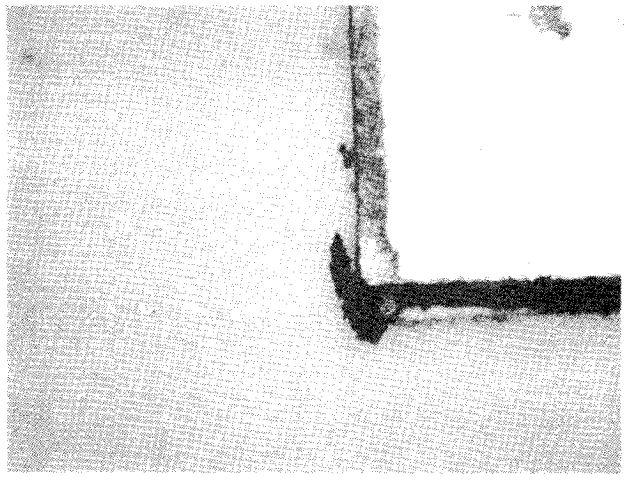

Fig. 5 Photograph of underside of 1 × 2 cm² cell.

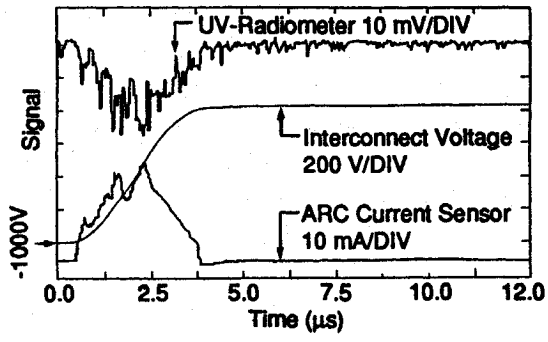

Fig. 6 Solar cell arc temporal evolution.

III. Electrical and Optical Characteristics of Solar Cell Arcs

The combined use of electrical and optical diagnostics for the detection of arcs produced an interesting correlation. Typical current and voltage traces derived from the arc sensors are shown in Fig. 6. The current sensor trace shows a discharge of approximately 2 μs in duration that is highly structured. The simultaneous trace for the voltage sensor corresponds, as expected, to a running integral of the arc current. For this specific measurement the cell bias voltage was −1000 V, and peak currents during the arc reached 30 mA. Note that the voltage trace indicates a reduction in the cell voltage from −1000 V to approximately −300 V at the termination of the arc. The arcs observed from these cells span a range of currents and cell voltage reductions. The arc current can be related to the cell voltage drop through the relation

$$\Delta Q = C\,\Delta V \tag{1}$$

where ΔQ is the total charge transferred in the arc, ΔV is the total voltage drop on the cell during the arc, and C is the capacitance of the arc sensor measurement system. Figure 7 shows the integral of the charge transferred in an arc as a function of the total voltage drop for a range of arc events. The slope of the line formed from the plot, 53 ± 0.05 pF, agrees quite well with the measured capacitance of the arc sensor system, 52 pF.

The solar cell biasing system included the capability to add additional capacitance to the cell to simulate the response of a much larger array of cells. This capacitance could be varied from the inherent capacitance of the system of approximately 78 pF to a total capacitance of nearly 800 pF. A significant observation of the arc electrical characteristics was that the arc duration was insensitive to added capacitance but that the arc current scaled linearly with added capacitance.

Arc data recorded simultaneously using both the arc current sensor and the UV radiometer reveal a remarkable correlation between the two phenomena. Figure 8 is a scaled overlay of arc temporal evolution as seen by both sensors. The sensors reproduce both the temporal duration of the arc as well as the fluctuations in arc intensity. Similarly, signal from the UV radiometer shows a linear correlation with voltage drop on the solar cell interconnect. These data are presented in Fig. 9 for two applied cell capacitances: 78 and 780 pF. Since arc current

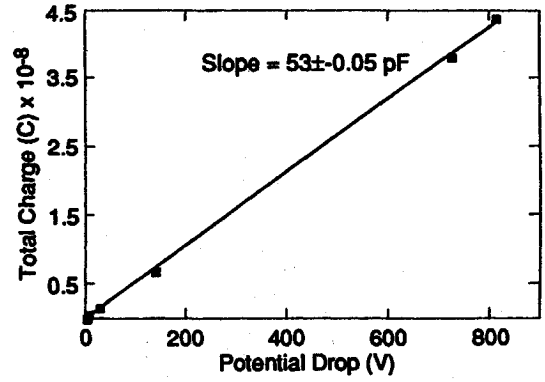

Fig. 7 Correlation of the measured charge dissipated in an arc event to the interconnect potential drop verifies the arc sensor capacitance.

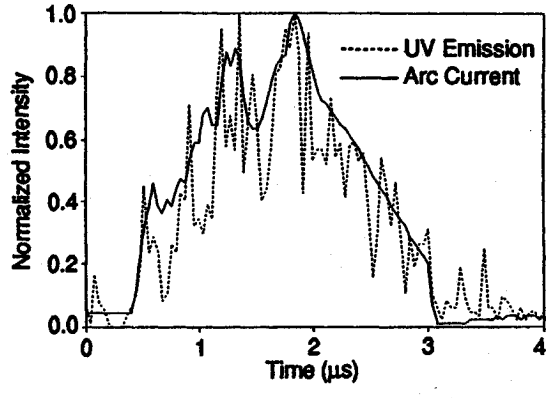

Fig. 8 Overlay of arc temporal evolution viewed by both arc current and UV light sensors.

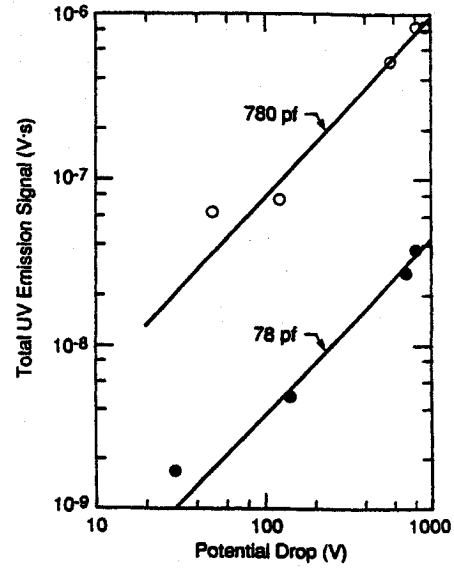

Fig. 9 Correlation of UV light emission with interconnect potential drop.

is also linearly correlated with cell voltage drop (Fig. 7), a linear correlation exists between arc current and optical emission from the arc. The correlation of arc current with UV emission intensity remains linear with interconnect voltage reduction at higher capacitances. However, the efficiency with which UV photons are produced changes with added capacitance. At a cell capacitance of 78 pF, UV photons are produced with an efficiency of 1.1×10^{-4} per electron transferred in the arc. When the cell capacitance is increased to 780 pF, the efficiency increases to a value of 2.3×10^{-4} per electron.

A. Arc Spatial Imaging

The use of an imaging system to monitor arc location played a key role in many of the conclusions drawn from our efforts. Images of arcs originating on the 1×2 cm^2 silicon cells showed that arcs were confined to the outer three edges of the cell. These edges were all characterized by a coverglass that extended beyond the edge of the cell by approximately 100 μm and the presence of excess adhesive extruded from the cell/coverglass interface. Figure 10 shows a typical arc observed at the lower edge of a cell. The spatial extent of the arc is approximately 500 μm in diameter.

In some instances two distinct arcs are observed spatially within a period that is characterized by a single arc pulse electrically. Since the gate duration on the camera intensifier is short (5 μs) compared with the period between arcs (typically 100 ms), it is unlikely that the camera simply observed two unrelated arc events occurring simultaneously. A more appropriate explanation is the triggering of a nearby arc site by the first arc event.

B. Arc Spectral Imaging

Spectra of solar cell arcs were recorded for the 1×2 cm^2 Spectrolab cells, as received. Figure 11 shows a spectrum of an arc recorded with a total system capacitance of 0.1 μF biased at −1000 V. Features occurring at 328 and 338 nm, respectively, are assigned to emission from atomic silver on the extremely strong $^2P_{1/2,3/2} - {}^2S_{1/2}$ transition. Other features are observed in the 220–240 nm region and at 273 nm. These cannot be conclusively assigned but may be due to molecular species. The observation of emission from Ag is significant, since all of the metallic surfaces of the solar cell are Ag-plated for bonding purposes.

C. Environmental Effects on Arcing

Our observations also indicated that the ambient environment of the solar cell had an impact on the apparent arcing rates. The previously noted cell conditioning effects are a component of these environmental effects. Figure 12 illustrates the impact of solar cell heating on the arcing rate. This heating is accomplished indirectly, through the radiant heat load placed on the thermally isolated cell by the plasma-neutralizing filament in the Kaufmann ion source. After thorough degassing of the solar cell in the UHV chamber (base pressure 2×10^{-9} Torr), the cell was subjected to both the radiant and plasma loading from the Kaufmann source. The data show a distinct decrease in arcing rate with exposure time. During this period the solar cell equilibrates to a temperature of 85°C.

Experiments were conducted to isolate the effects of thermal processing from plasma exposure. After cycling the cell back to atmospheric pressure with room air, the cell was again placed in the vacuum chamber for testing. In previous cycling of this sort the cell arcing rate had returned to its initial pre-exposure value. The cell was again exposed to the Kaufmann source operating in a manner that did not allow plasma production. This technique allowed for the normal radiative heating of the cell without the corresponding plasma exposure. In a series of tests the cell was heated in vacuum for a fixed period of time, following which plasma exposure was initiated and the cell arc rate was determined. Figure 12 also shows the results of such an experiment for which the cell was heated for periods of 45

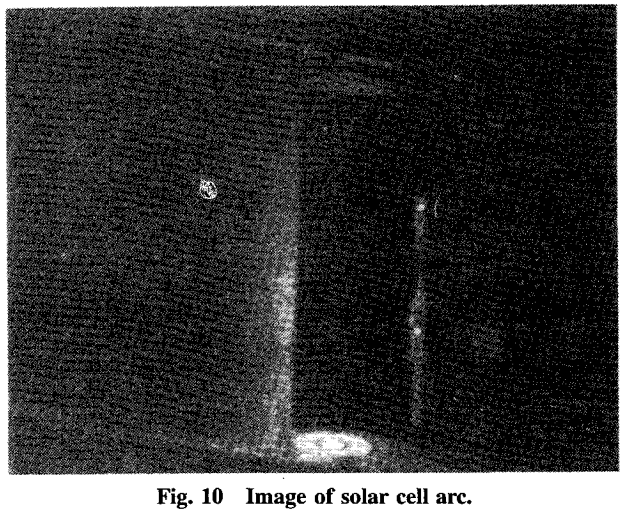

Fig. 10 Image of solar cell arc.

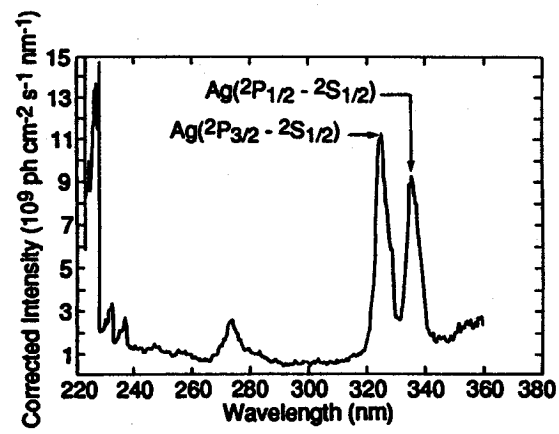

Fig. 11 Emission spectrum from high applied capacitance solar cell arc.

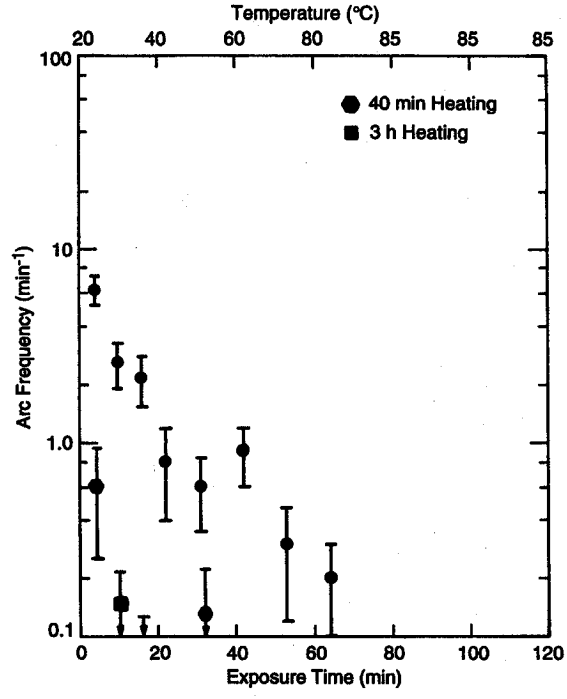

Fig. 12 Conditioning of solar cell arc frequency with plasma exposure time, showing impact of cell heating on measured arcing rates.

min and 3 h before arc rate measurements. The data reveal a reduction in the initial arc rate of the cell by a factor of 10 for 45-min exposure and greater than a factor of 100 for 3-h exposure. In fact, after 3 h of exposure the cell arc rate fell below the practical detection limit of 0.1 arcs per minute at an applied bias of −1000 V. Once thermally conditioned and confined to a vacuum environment, the arc rate for these cells remained below detection limits for periods ranging from several days to weeks. Exposure to room air immediately established the pre-exposure arcing behavior, whereas exposure to comparable amounts of pure O_2, N_2, Ar, or CO_2 had no impact on the measured arcing rates.

The data cited earlier indicate that an airborne constituent common to both the natural air and UHV environment may play a role in cell conditioning. Furthermore, the evidence from the thermal processing studies shows that the contaminant is tightly bound to the cell, since a significant temperature increase is required to effect its removal. A strong candidate for the interacting species is H_2O. Clearly common in room air, H_2O is also the primary contaminant in UHV chambers, albeit at a much reduced level. These results are confirmed by mass spectrometer analysis of the UHV chamber background gas, which is largely a mixture of H_2O and CO_2. The background water vapor concentration in the chamber is enhanced by approximately a factor of 100 during Kaufmann source operation, to a pressure of 2×10^{-7} Torr. The enhancement is a result of thermal desorption of water from the walls by the charge neutralization filament heating. By comparison, the equilibrium vapor pressure of H_2O at room temperature is approximately 18 Torr. The relative amounts of H_2O present in these two regimes account for the disparity in deconditioning times for the cell.

Confirmation of the role played by H_2O vapor was obtained by enhancing the exposure of the cell to the vapor in a controlled manner. In these experiments the chamber was equipped with a variable leak valve that introduced a thoroughly degassed flow of water vapor into the test chamber. Cells were conditioned and held at 85°C until the previously noted reduced arcing rate was obtained. The cell was then subjected to successive dosings by H_2O at a fluence of 2.5×10^{-4} Torr-min, i.e., the chamber was brought to a pressure of 5×10^{-5} Torr for a period of 5 min. Between each exposure the plasma source was activated, and the cell arcing rate was measured. The data obtained from these successive exposures are plotted in Fig. 13. The data show a progressive increase in the cell arcing rate from the conditioned state to an asymptotic level characteristic of the cell before conditioning. These data show clear evidence of the role played by H_2O in promoting arcing. Note that the interaction of the water vapor is with the cell and not with the plasma, since simultaneous exposures were not employed in these measurements. Furthermore, the data support the notion that the water is held in depth within a component of the cell. This is likely because the desorption rate of water from the surface of the cell is fast compared with the observed conditioning times.

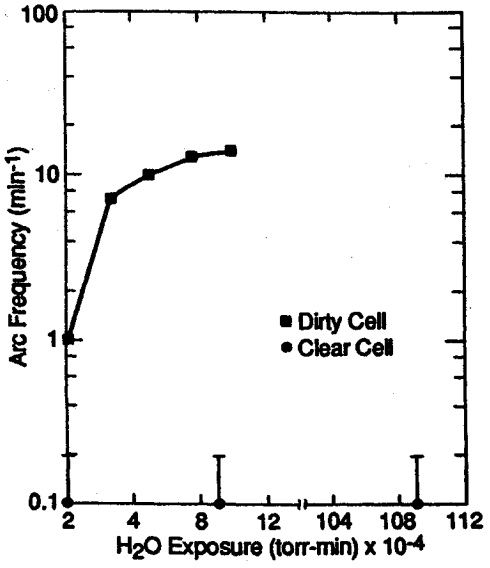

Fig. 13 Effect of water vapor exposure on observed arc rate.

The role of the extruded adhesive layer found at the silicon/coverglass/plasma triple junction was also illustrated in our measurements. A solar cell that had been modified to remove the extruded adhesive (using a solvent) was subjected to the same set of experiments described earlier for the unmodified cells. Cells that had been modified in this manner showed none of the conditioning behavior observed for as-manufactured cells. From the inception of testing these cells exhibited an arc rate below the measurement threshold. Furthermore, treatment of the cells with additional water vapor did not raise the arcing rate. In later measurements, cells that had been processed to remove excess adhesive using mechanical abrasion were tested. These cells still exhibited considerable conditioning effects. These differences may be due to the presence of small hairlike adhesive filaments remaining from the mechanical abrasion process.

D. Plasma Scaling

Arcing rate measurements on PIX II had shown a correlation with plasma density. A scaling of arcing rate with plasma density is also predicted in the theory developed by Cho and Hastings[19] when the plasma flux is low. The UHV chamber and Kaufmann plasma source were employed in their usual configuration. The test article was an array of six Spectrolab 1×2 cm^2 cells mounted on a Kovar plate. These cells were used without removing the adhesive from the edges of the cells but were conditioned by prolonged plasma exposure at a bias of −1000 V. Tests were conducted at a bias of −1000 V. The conditioning process was continued until the arcing rate ceased to change for several observation periods. The plasma scaling experiments were conducted by varying the operating pressure and ionization characteristics of the Kaufmann source. The planar Langmuir probe was used to determine the plasma density. Figure 14 shows the variation in arcing rate obtained as a function of plasma density from 2.5×10^5 to 6.6×10^6 cm^{-3}. The arcing rate shows a linear correlation with plasma density over this range, as evident from the least-squares line of Fig. 14.

E. Arc Threshold

As pointed out by Ferguson,[3] an actual threshold for arcing has not been measured due to the difficulties in maintaining constant experimental conditions for long observation periods. Our observations of arc rate sensitivity to exposed water contaminated adhesive indicate that the most uncontrollable experimental parameters are the surface cleanliness and condition.

Steady-state arc frequency-voltage characteristics were determined for two six-cell arrays. One array was assembled with silicon cells without removing the excess coverglass adhesive;

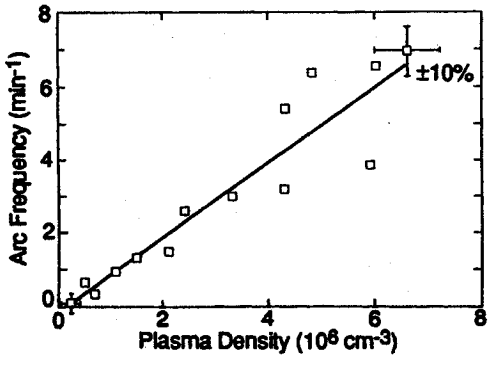

Fig. 14 Scaling of solar cell array arcing rate with plasma density at a bias of −1 kV.

the second array consisted of solar cells from which the excess adhesive had been removed. The results shown in Fig. 15 were obtained following 1 h of −1 kV conditioning in our standard plasma. The measured arc rate at any point was stable over a period of 30 min and repeatable within the error bars exhibited. The power dependence on voltage is approximately 7 ± 0.5 for both sets of data. In neither case was a true threshold, i.e., exhibited by a rapid arc rate increase, observed. The lower voltage measurements are limited by simple statistics to reach meaningful measurement uncertainties and continuous operation life of the Kaufmann source.

IV. Theory

A theory for arcing on high-voltage solar cells has been developed in a series of papers.[15,19,20] The theory has been developed on the basis of detailed particle in cell simulations of a model of the triple junction. The theory includes dielectric inclusions to simulate extruded adhesive on the interconnector. The theory suggests the following physical picture:

1) The ambient ions charge the dielectric front surface to the steady-state potential ≃ 5 V, where 5 eV is the kinetic energy of the incoming ions with the orbital velocity in LEO. Therefore, at the steady state given by the ion charging, a strong electric field of $E \simeq V/d$ is created at the triple junction, where V is the bias potential on the conductor and d is the thickness of the dielectric.

2) After the electric field reaches the value of $E = V/d$ at the triple junction, if there is an emission site (on the adhesive) with a high field enhancement factor[20] β (β is the nominal height/width of the emission site), on the conductor surface near the triple junction, then electrons can be emitted profusely and can charge the side surface. The functional dependence of the current density on the electric field at the adhesive emission site E_e is

$$j_{ec} = A(\beta^2 E_e^2) \exp\left(-\frac{B}{\beta E_e}\right) \tag{2}$$

where A and B are constants determined by the work function of the surface ϕ_ω. This charging due to enhanced field electron emission (EFEE) charges the side of the dielectric positive and can therefore enhance the electric field at the triple junction. It can develop very rapidly because of the strong exponential dependence of the current on the electric field. Near the threshold for field-assisted electron emission, when the electric field doubles, the emission current increases by 10 orders of magnitude (see Ref. 19). This incident current can desorb a significant amount of neutral gas from the surface and create a dense neutral cloud as high as 10^{21} m^{-3} over the surface. The electron current flowing through the neutral cloud can lead to a discharge like a surface flashover. Even if there is not a dense neutral cloud created over the dielectric, the electric field just over the surface may increase to the point where dielectric breakdown of a thin layer along the side of the dielectric occurs. For an initial conductor voltage of 500 V across a coverglass of 150 μ, the initial electric field imposed along the edge of the coverglass is 3.3×10^6 V/m. As discussed in the previous sections, the coverglasses are held on with an adhesive that can have a dielectric breakdown strength as low as 2×10^7 V/m. Hence the electric field along the side of the coverglass only needs to be enhanced by an order of magnitude for dielectric breakdown of the adhesive or surface flashover of desorbed neutral gases to occur.

Once the charging time of the dielectric coverglass is known, the arcing rate for a given solar array can be calculated, assuming that it takes a negligible amount of time for the ionization of neutral gases or for dielectric breakdown to occur relative to the field buildup time. The arcing rate is then defined as the inverse of the time that is necessary to build up the electric field and charge the surface with ions. The time between arcs is therefore given by

$$\tau_{arc} = \tau_{efee} + \tau_{ion} \tag{3}$$

where τ_{efee} is the charging time due to enhanced field emission electrons and τ_{ion} is the charging time due to ions. In Ref. 19, the charging times were calculated numerically using the particle in cell simulation. In Ref. 20 a semianalytic formula was derived for the arcing rate.

The application of the semianalytic formula from Ref. 20 for a Spectrolab 1 × 2 cm cell without removing excess coverglass adhesive is shown in Fig. 16. For the calculations in Fig. 16 the emission site density was chosen as $n_{cs} = 1 \times 10^5$ m^{-2} with an exponential distribution of field enhancement factors with average value $\beta_p = 120$. The plasma conditions were the same as in Fig. 15. The results in Fig. 16 show good agreement with the experimental data up to about a kilovolt. They predict a quasithreshold when the charging process is exponentially slow. The lower parts of the curves occur when the enhanced field electron emission charging is the slowest charging process in the system. The arc rate dependence on voltage here is exponential and enables a quasithreshold voltage to be defined with a small uncertainty. The threshold voltage therefore can be

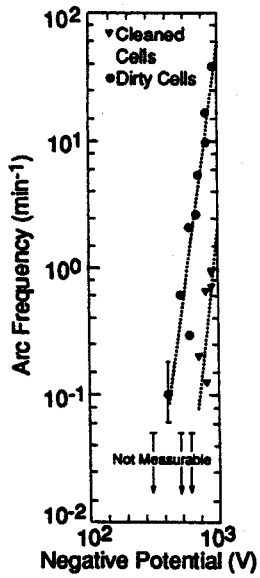

Fig. 15 Steady-state arc frequency, voltage characteristics.

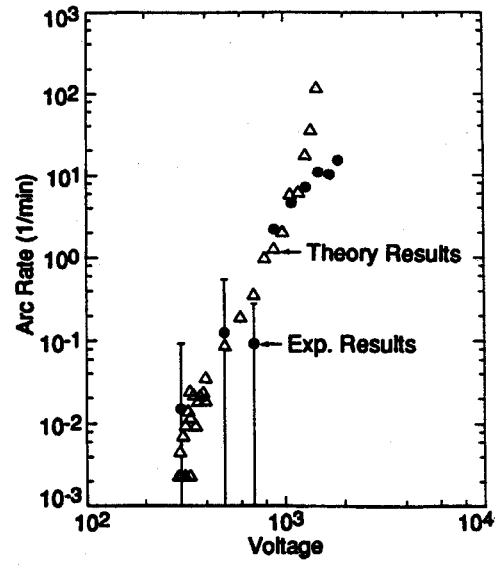

Fig. 16 Comparison of theory calculation with experimental measurements of solar cell arcing rates.

defined as the voltage at which the arc rate is decaying very rapidly. The upper parts of the arc rate curves become more dominated by the ion recharging time. The fact that the arc rate scales with the density for the higher voltages can also be explained from the dominance of the ion recharging time, since this scales inversely with the density. Above a kilovolt, the theory overpredicts the experimental data. This may be due to the neglect of the finite rate of neutral reabsorption on the adhesive sites after an arc.

V. Discussion and Conclusions

The arc characterization data suggest that a significant mode of solar cell arcing is through dielectric breakdown of excess adhesive at the coverglass/silicon interface. The distribution of adhesive in this region is irregular. Hence, it is somewhat difficult to specify the mechanism by which H_2O vapor influences arcing behavior. However, a possible mechanism for the process can be postulated by invoking the presence of a gradient in the dielectric strength of the adhesive barrier formed between the biased solar cell and the space plasma. The gradient is driven by the interaction of adsorbed water vapor with ionic impurities in the adhesive. Water-saturated adhesive acts as a conductor, allowing current from the plasma to pass through the cell under the influence of the bias voltage. Under vacuum, water is desorbed from the adhesive at the adhesive/vacuum interface, forming a thin dielectric layer that must hold off the cell bias. At select sites the voltage gradient exceeds the breakdown strength of the film resulting in an arc. As water continues to desorb from the cell, the thickness of the water-depleted dielectric layer at the interface increases until it meets the silicon. At these greater film thicknesses sufficient dielectric strength exists to support the cell bias and arcing ceases.

The role of temperature in the cell arcing process is twofold. Its primary role is in enhancing the rate of diffusion of adsorbed water vapor from within the adhesive to the vacuum interface, where it rapidly desorbs, i.e., the rate-limiting step in water removal from the adhesive is diffusion in the solid. A secondary effect of a temperature increase is a reduction in the equilibrium water concentration supported in the adhesive. This conclusion is confirmed by the observation that reduced arcing rates are maintained for many days once the cell has been cooled to room temperature in vacuum after the water vapor has been desorbed from the adhesive.

Two distinct conclusions can be derived from the optical emission and electrical characteristics data. The first conclusion is that the optical emission is derived from a region that is a thin target for the electrons emitted from the arc. In a thickly absorbing region the optical emission would scale with the discharge power, which is the product of instantaneous current and voltage. The linear correlation of discharge current with photon intensity confirms the thin gas limit.

The second conclusion is that some fraction of the emitting species is produced from electron excitation of neutral species ejected from the arc site. This is confirmed by the prevalence of emission from Ag in the arc emission spectra and is also suggested by the change in photon production efficiency with discharge capacitance. The production of a locally higher gas density by the higher energy arc, which remains thin for electron excitation, would result in an apparent increase in the photon production efficiency while maintaining the linearity of the emission with arc current. The observation that arc current, but not arc duration, scales approximately linearly with added capacitance also supports the rarified plume interpretation. These conclusions advance the idea that arc emission can be used as a quantitative measure of arc strength. Furthermore, optical emission from arcs could be used in an imaging configuration to remotely monitor arc rate, strength, and location on large space structures in orbit.

The observation of multiple arc sites within a single camera image (5-μs period) provides a dramatic example of the spatial extent over which the arc can have influence. It would be reasonable to expect that the radius over which this triggering event would occur could be related to the energy dissipated in the arc, since the arc spatial extent is determined by the range over which neutral and charged species are ejected from the substrate. Hence, the inherent capacitance of that portion of the array coupled to the arc may have an impact on arc spatial extent through the triggering of arcs on other, electrically isolated portions of the array. This problem has been recently addressed by Vaughn et al.,[21] who have developed a model for coupling between adjacent sites that incorporates plume expansion and agrees well with laboratory experiments.

Numerous laboratory and flight experiments have measured the voltage dependence of the arc frequency and attempted to identify an arc threshold. Although the power dependence has varied by factors of two to three, most experimenters agree that at potentials more positive than -200 V arcs are not observed. Our investigations confirm that the surface condition plays a critical role in determining the arc frequency voltage characteristic of the array; however, the effect on arc threshold is not as clear. The fast rise in the arc frequency associated with the onset of a new phenomenon was not exhibited in our data. The data indicate that the arc frequency declines at low voltages with the same V^7 power dependence as observed at high voltage. The "apparent" threshold, defined as the voltage below which arcs are not observed in a reasonable experiment time, can be discussed but is linked to the surface conditioning. Without preconditioning we have observed solar cell arcing at potentials more negative than -150 V. These arcs are typically transitory and in the time frame of tens of minutes decrease below reasonable statistical detection. Following conditioning at -1 kV, we would quote an apparent threshold of -300 V for a solar array with exposed adhesive and -500 V for a solar array without exposed adhesive. Finally, the close agreement of the theory with the data confirm the importance of the adhesive extrusions and neutral gas on the arcing. It suggests, as confirmed by experiments, that efforts to reduce both will reduce the arc rate.

Acknowledgments

This effort was sponsored by NASA Lewis Research Center under Contract NAS3-25797. The authors would like to thank the following people for their roles in the conduct of this effort: Alan Gelb, Herbert Cohen, and B. David Green for review of the technical effort; Mark Horenstein of Boston University for his helpful discussions and guidance of Ed Aifer; and Mark Allen for his help in the use of the imaging CCD camera system. We would also like to thank David Snyder, Dale Ferguson, and Barry Hillard for their support of the effort at NASA Lewis Research Center. In addition, we would like to acknowledge the assistance of David Hardy, Don Guidice, and Paul Severance at the Geophysics Directorate of the Air Force Phillips Laboratory, Raymond di Gaston of Vitro Corporation, and Jim Abreck of Spectrolab Inc. for supplying us with test solar cells.

References

[1] Grier, N. T., "Experimental Results on Plasma Interactions with Large Surfaces at High Voltages," NASA TM-81423, Jan. 1980.

[2] Grier, N. T., "Plasma Interaction Experiment II: Laboratory and Flight Results," NASA CP-2359, March 1985, pp. 333–349.

[3] Ferguson, D. C., "The Voltage Threshold for Arcing for Solar Cells in LEO—Flight and Ground Test Results," NASA TM-87259, March 1986.

[4] Miller, W. L., "An Investigation of Arc Discharging on Negatively Biased Dielectric-Conductor Samples in a Plasma," NASA CP-2359, March 1985, pp. 367–377.

[5] Thiemann, H., and Bogus, K., "Anomalous Current Collection and Arcing of Solar-Cell Modules in a Simulated High Density Low-Earth-Orbit Plasma," *ESA Journal*, Vol. 10, No. 1, 1986, pp. 43–57.

[6] Snyder, D. B., "Discharges on a Negatively Biased Solar Array in a Charged Particle," NASA CP-2359, March 1985, pp. 379–388.

[7] Snyder, D. B., "Characteristic of Arc Currents on a Negatively Biased Solar Cell Array in a Plasma," NASA TM-83723, July 1984.

[8] Thiemann, H., Schunk, R. W., and Bogus, K., "Where Do Negatively Biased Solar Arrays Arc?," *Journal of Spacecraft and Rockets,* Vol. 27, No. 5, 1990, pp. 563–565.

[9] Stevens, N. J., "Environmentally Induced Discharges on Satellites," NASA TM-82849, May 1982.

[10] Fujii, H., Shibuya, Y., Abe, R., Ijichi, K., Kasais, R., and Kuriki, K., "Laboratory Simulation of Plasma Interactions with High Voltage Solar Arrays," *Proceedings of the 15th International Symposium on Space Technology and Science,* ISAS, Tokyo, 1986.

[11] Kuninaka, H., "Qualitative Experiment with Arc Discharges on Negatively Biased Solar Cells," *Journal of Spacecraft and Rockets,* Vol. 27, No. 6, 1990, pp. 665–668.

[12] Thiemann, H., and Bogus, K. P., "High-Voltage Solar Cell Modules in Simulated Low-Earth-Orbit Plasma," *Journal of Spacecraft and Rockets,* Vol. 25, No. 4, 1988, pp. 278–285.

[13] Kennerud, K. L., "High Voltage Solar Array Experiment," NASA CR-121280, March 1974.

[14] Parks, D. E., Jongeward, G., Katz, I., and Davis, V. A., "Threshold-Determining Mechanisms for Discharges in High Voltage Solar Arrays," *Journal of Spacecraft and Rockets,* Vol. 24, No. 4, 1987, pp. 367–371.

[15] Hastings, D., Weyl, G., and Kaufmann, D., "A Simple Model for the Threshold Voltage for Arcing on Negatively Biased Solar Arrays," *Journal of Spacecraft and Rockets,* Vol. 27, No. 4, 1990, pp. 539–544.

[16] Weyl, G., Hastings, D., Kaufmann, D., and Green, B. D., "Arcing in Negatively Biased Structures in Low Earth Orbit," Physical Sciences, Inc., PSI-2057/TR-889, Andover, MA, Dec. 1988.

[17] Frederickson, A. R., Cotts, D. B., Wall, J. A., and Bouquet, F. L., *Spacecraft Dielectric Material Properties and Spacecraft Charging,* Vol. 107, Progress in Astronautics and Aeronautics, AIAA, New York, 1986, pp. 9, 10.

[18] Wood, B. E., Bertrand, W. R., Bryson, R. J., Seiber, B. L., Falco, P. M., and Cull, R. A., "Surface Effects of Satellite Material Outgassing Products," *Journal of Thermophysics and Heat Transfer,* Vol. 2, No. 4, 1988, pp. 289–295.

[19] Cho, M., and Hastings, D. E., "Dielectric Charging Processes and Arcing Rates of High Voltage Solar Arrays," *Journal of Spacecraft and Rockets,* Vol. 28, No. 6, 1992, pp. 698–706.

[20] Hastings, D. E., Cho, M., and Kuninako, H., "The Arcing Rate for a High Voltage Solar Array: Theory, Experiments and Predictions," *Journal of Spacecraft and Rockets,* Vol. 29, No. 4, 1992, pp. 538–554.

[21] Vaughn, J. A., Carruth, M. R., Jr., Katz, I., and Jongeward, G., "Extrapolation of Electrical Breakdown Currents from the Laboratory to Space Station," AIAA Paper 92-0822, Jan. 1992.

Alfred L. Vampola
Associate Editor